Sensors & Actuators: B. Chemical 371 (2022) 132591

Contents lists available at ScienceDirect

Sensors and Actuators: B. Chemical

journal homepage: www.elsevier.com/locate/snb

Dual-quenching electrochemiluminescence system based on resonance energy transfer from gold dendrite@polypyrrole core–shell nanoparticles enhanced g-C_3N_4 to ZnONFs@PDA-sCuO for procalcitonin immunosensing

Tengfei Shi [a], Lihua Hu [a,*], Jiye Chen [a], Qianqian Cui [a], Hao Yu [a], Yuyang Li [a,*], Dan Wu [a], Hongmin Ma [a], Qin Wei [a], Huangxian Ju [a,b]

[a] Collaborative Innovation Center for Green Chemical Manufacturing and Accurate Detection, Key Laboratory of Interfacial Reaction & Sensing Analysis in Universities of Shandong, School of Chemistry and Chemical Engineering, University of Jinan, Jinan 250022, China
[b] State Key Laboratory of Analytical Chemistry for Life Science, School of Chemistry and Chemical Engineering, Nanjing University, Nanjing 210023, PR China

ARTICLE INFO

Keywords:
ECL-RET
G-C_3N_4-AuD@PPy
ZnONFs@PDA-sCuO
Procalcitonin detection

ABSTRACT

This work presents a dual-quenching electrochemiluminescence resonance energy transfer (ECL-RET) immunosensor on account of the double quenching effects of polydopamine coated ZnO nanoflowers (ZnONFs@PDA) loaded with small-sized copper oxide nanoparticles (sCuO), named ZnONFs@PDA-sCuO, towards gold dendrite@polypyrrole core–shell nanoparticles (AuD@PPy) enhanced g-C_3N_4 (g-C_3N_4-AuD@PPy) for sensitive analysis of procalcitonin (PCT). To be specific, AuD@PPy with core-shell structure were loaded onto g-C_3N_4 to enhance the emission performance of g-C_3N_4. In addition, the ultraviolet absorption spectra of ZnONFs@PDA and sCuO showed considerable overlap with the ECL emission spectra of g-C_3N_4 appropriately. So sCuO and ZnONFs@PDA were combined and designed as an efficient dual-quencher of ECL luminescence of g-C_3N_4 by RET interaction. The biosensor showed superior linear detection range from 0.00005 to 50 ng mL^{-1}, with a sensitive detection limit of 17.2 fg mL^{-1} (S/N = 3). It is worthy to note that a new type ECL-RET couple made up of g-C_3N_4-AuD@PPy (donor) and ZnONFs@PDA-sCuO (acceptor) was developed to construct a sandwich ECL biosensor for PCT detection. The studied immunosensor had satisfactory sensitivity, specificity and reproducibility, indicating the proposed sensing method could provide a good technical means and theoretical basis for the diagnosis of serious diseases.

1. Introduction

Procalcitonin (PCT), normally produced by thyroid C cells, is a peptide precursor of hormone calcitonin [1]. In the case of systemic bacterial infection, many non-thyroidal cells also produce PCT, and serum levels of PCT increase sharply within a few hours compared with those in the serum of healthy individuals, so PCT concentration is primarily used to recognize severe bacterial inflammation, fungal infections and autoimmune diseases [2–5], which is also especially authoritative in the diagnosis of sepsis [6], acute-on-chronic liver failure (ACLF) [7] and bacterial pneumonia [8]. However, at present the commonly used methods for PCT detection have many shortcomings, such as high sample dosage, low sensitivity, specialized equipment and time-consuming process. Therefore, it is of critical concern to explore new detection schemes with high efficiency, easy operation, low-cost and ultra-high sensitivity to detect PCT.

During the process of ECL, the luminous signal comes from the annihilation of the excited state matter, which is resulted from the electron transfer reaction products of species generated at electrodes [9]. Meanwhile, a luminescence process was involved in an electron gain and loss reaction of reagents [10]. As a new burgeoning method, ECL has the advantages of glorious sensitivity, weak background signal, rapid response and plain instrument, and thus be extensively studied by researchers [11–14]. ECL-RET method is realized by means of energy transfer between a donor and an acceptor on the nanometer scale. Specifically, it requires a well-matched overlapping between the UV-Vis absorption spectrum of the acceptor and the ECL spectrum of the donor [15–17]. Therefore, the key point of constructing ECL-RET immunosensors is how to design a novel pair of acceptor and donor to improve the sensing performance.

* Corresponding authors.
E-mail addresses: hulihua1206@163.com (L. Hu), chm_liyy@ujn.edu.cn (Y. Li).

https://doi.org/10.1016/j.snb.2022.132591
Received 10 April 2022; Received in revised form 26 August 2022; Accepted 28 August 2022
Available online 6 September 2022

Coincidentally, graphite phase carbon nitride (g-C_3N_4) with the advantages of nontoxicity, excellent biological compatibility, outstanding stability and metal-free construction, have been broadly used in photochemical [18], electrochemical catalysis [19], fluorescence [20] and other fields. As an emerging ECL luminophore, g-C_3N_4 has good luminescence behavior. However, its luminescence behavior cannot be stable for a long time [21–23]. In biological signal enhancement and surface functionalization, gold nanoparticles (Au NPs) have been broadly applied because of the features in electronic transmission, photology, catalysis, and biological compatibility [24]. According to the literature reports, the ECL signals of many luminescent materials, such as luminol [25], quantum dots [26] and $Ru(bpy)_3^{2+}$ [27] can be effectively enhanced by Au NPs. While in comparison with the citrate-wrapped Au NPs, polypyrrole modified gold dendrite (AuD@PPy) nanocomposites with core-shell structure have been verified to have enhanced catalytic durability, which was due to the shielding action resulted from the polypyrrole shell [28]. In addition, because of the porous nature of the polypyrrole thin film, small molecules are still allowed to contact with the internal gold dendrite surface [29]. So AuD@PPy nanocomposites were compounded with g-C_3N_4 in hopes of improving its luminous properties and further increasing the sensitivity and stability of the biosensor.

Zinc oxide is a sort of metal oxide semiconductor, which has the characteristics of highly electron mobility, excellent long-term stability, good biocompatibility and morphological diversity [30,31]. Especially, ZnO has diversified structure, which has great underlying application in the design of ECL sensor [32]. The high specific surface area of flower-shaped ZnO makes it particularly suitable for loading object. Therefore, it is feasible to use ZnO nanoflowers (ZnONFs) as an efficient carrier to prepare the secondary antibody markers in a sandwich-type ECL immunosensing system. CuO nanoparticles have significant characteristics of salient chemical stability, controllable scale, and extended light absorption range, which are widely used in optical, electrical, semiconductor and electrode materials [33,34]. What's more, the ultraviolet absorption spectra of small-sized copper oxide nanoparticles (sCuO) were found to have some degree of overlap with the ECL emission spectra of g-C_3N_4 effectively. So sCuO could be expected to effectually extinguish the ECL signal intensity of g-C_3N_4 by resonance energy transfer interaction.

Polydopamine (PDA), as a kind of multifunctional material with good biocompatibility, has aroused extensive attention in biology and energy-related fields [35,36]. In the molecular chain of this melanin-like biopolymer, numerous amino and hydroxyl endow PDA with strong adhesion, and ease of functionalization [37]. PDA has been proved to be a kind of ECL quenching agent used for building sensing strategies [38]. Therefore, it is proposed here to use PDA as a bridge to realize the high-efficiency load of sCuO nanoparticles and antibody molecules onto the surface of ZnO nanoflowers to obtain a high-efficiency ECL quenching probe (ZnONFs@PDA-sCuO).

Herein, in view of the outstanding ECL property of the AuD@PPy functionalized g-C_3N_4 (g-C_3N_4-AuD@PPy) and the super quenching ability of ZnONFs@PDA-sCuO, a quenching type ECL biosensor based on RET mechanism from the newly designed g-C_3N_4-AuD@PPy (donor) to ZnONFs@PDA-sCuO (acceptor) was manufactured for PCT determination. The selectivity, repeatability and stability of the biosensor are satisfactory. Moreover, the prepared ECL sensor achieved a wide detection range (0.00005–50 ng mL^{-1}) and a low detection limit (17.2 fg mL^{-1}) for PCT analysis. This work can provide a new theoretical basis and method reference for the clinical detection of other biomarkers.

2. Experimental section

2.1. Preparation of g-C_3N_4-AuD@PPy

The water dispersion of g-C_3N_4 was synthesized based on the literature [39] and the specific process was stated in the Supplementary Material. AuD@PPy was synthesized according to known methods [28]. In brief, pyrrole (0.4 g) was dissolved in deionized water (20 mL). Then 0.01% (g/g) $HAuCl_4$ solution (200 mL) was added and reacted at 30 ℃ for 2 h. The product was collected through centrifugation. Finally, the collected product was dissolved in deionized water to form AuD@PPy aqueous solution.

0.2 g of g-C_3N_4 was dispersed in 15 mL of deionized water. Then 3 mL of AuD@PPy aqueous solution was added and the reactants were stirred overnight. Subsequently, g-C_3N_4-AuD@PPy nanocomposites were obtained through centrifugation.

2.2. Synthesis of ZnONFs@PDA-sCuO-Ab_2

ZnONFs were synthesized by PVP-assisted coprecipitation method [40] and the specific process was stated in the Supplementary Material. Next, ZnONFs (60 mg) and dopamine hydrochloride (12 mg) were dissolved in Tris-HCl solution (60 mL) and stirred overnight. Finally, ZnONFs@PDA was obtained after 4 times of centrifugal rinsing with deionized water and overnight vacuum drying at 50 °C.

The small-sized copper oxide nanoparticles (sCuO) were synthesized through a quick-precipitation technology [41] and the specific experimental procedure was stated in the Supplementary Material. Then ZnONFs@PDA (5 mg) and sCuO (10 mg) were added to deionized water (30 mL), reacted under stirring at 25 ℃ thoroughly for 12 h. The solid was enriched by a centrifuge. After vacuum drying, ZnONFs@PDA-sCuO was obtained. Then Ab_2 (100 μL) and ZnONFs@PDA-sCuO (5 mg) were mixed in the phosphate buffered saline (PBS) solution (1 mL) and incubated at 4 °C for 12 h. The solid (ZnONFs@PDA-sCuO-Ab_2) was obtained after centrifugation and washing with PBS solution for three times.

2.3. Fabrication of the sandwich ECL immunosensor

The preparation process of the sensor is relatively simple (Scheme 1). Before using, the bare glassy carbon electrode (GCE) of 4 mm diameter was burnished with alumina slurry (0.3 μm and 0.05 μm) to obtain a glossy and apinoid surface. After target solution of g-C_3N_4-AuD@PPy (6 μL) was dropped on the cleaned GCE and allowed to dry, 6 μL Ab_1 was assembled by complexation between NH_2 groups of Ab_1 and Au, allowed by bovine serum albumin (BSA) (3 μL, 0.1 wt%) to take up the nonspecific adsorption sites. Thereafter, a series of different concentrations of PCT (6 μL) were spread onto the modified electrode, and kept in a moist state at 4 °C for 1.5 h. Lastly, the quench-type ECL immunocomplex was fabricated after the immune recognition binding of 6 μL ZnONFs@PDA-sCuO-Ab_2 bioconjugates, followed by storing at 4 °C for later use. In the above construction process, the as-prepared electrode was softly rinsed with PBS solution after each modification step to remove weakly-bound components.

2.4. ECL measurements

The three-electrode system was applied to investigate the ECL signal, and the ECL response of the modified electrodes was measured in 10 mL PBS solution. The following regulation parameters should be adjusted during measurement: the scan rate of 100 mV s^{-1}, the working potential ranging from − 1.5–0 V and the voltage of 700 V for the photomultiplier tube.

3. Results and discussion

3.1. Material characterization

The morphologies and size of the as-synthesized materials were mainly characterized by electron microscopy technologies. Fig. 1 showed the representative images. After ultrasonic stripping, g-C_3N_4 showed an ultra-thin nanosheet structure in the micron scale (Fig. 1A).

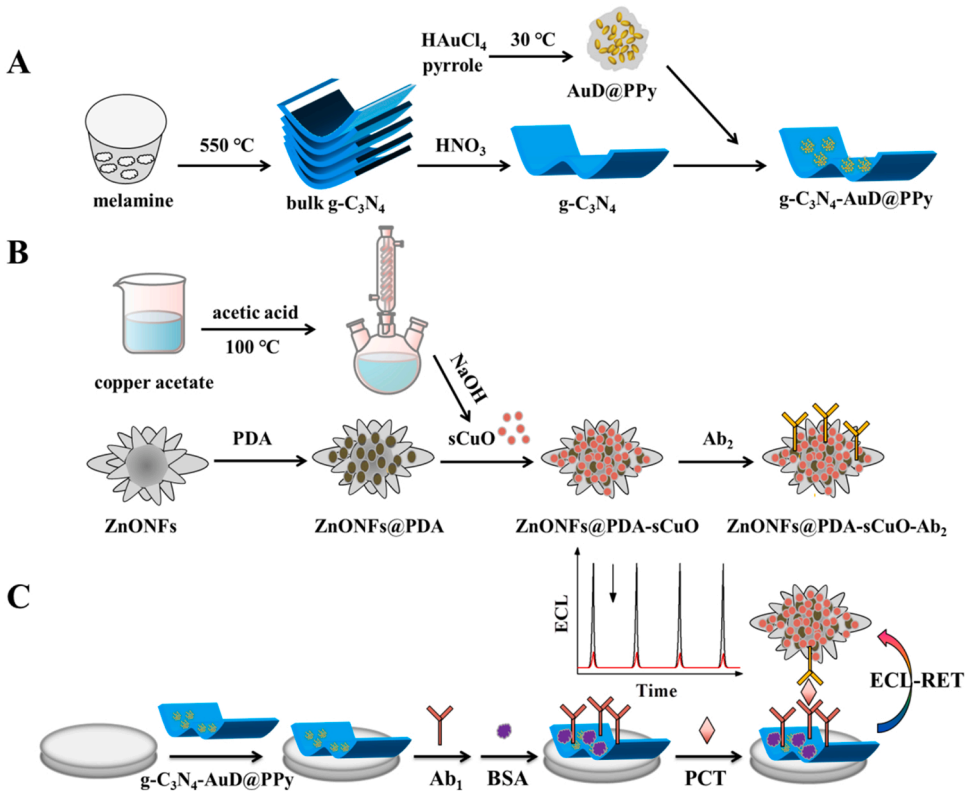

Scheme 1. Synthetic methods of the g-C_3N_4-AuD@PPy and ZnONFs@PDA-sCuO-Ab_2 and construction process of sensing system.

In addition, transmission electron microscopy (TEM) image of AuD@PPy core-shell nanocomposites demonstrated irregular sphere appearance with a size of about 30 nm (Fig. 1B). The high-resolution TEM (HRTEM) image of AuD@PPy nanocomposites shows that the crystal spacing of AuD@PPy nanocomposites was about 0.235 nm, corresponding to the (111) crystal surface of typical gold nanoparticles. Moreover, AuD@PPy was loaded on the interface of g-C_3N_4 nanosheet, which provided favorable evidence for the efficient synthesized of g-C_3N_4-AuD@PPy (Fig. 1D). The internal molecular structure of composite materials was further indicated by X-ray diffraction (XRD) (Fig. 1E). Curve a showed the XRD pattern of g-C_3N_4. The peak at 26.50° corresponds to the (002) plane of g-C_3N_4 (JCPDS Card No.87–1526). When loaded with AuD@PPy, the new peaks at 38.18°, 44.37°, 64.55° and 77.54° appeared (curve b), which can be assigned to the Au (111), (200), (220), (311) plane, respectively (JCPDS Card No. 89–1526), proving that g-C_3N_4-AuD@PPy luminous substrate was successfully synthesized.

The TEM image of sCuO revealed that the product consisted of spherical particles with a regular morphology. The average particle diameter was about 8 nm (Fig. 1F). The scanning electron microscopy (SEM) image of ZnO nanoflowers in Fig. 1G showed a multi-petal flower shape, and a size of about 2 μm. After in-situ polymerization of DA, the surface of ZnONFs was obviously wrapped by PDA layer (Fig. 1H). As shown in Fig. 1I, a lot of sCuO nanoparticles were bonded to the surface of ZnONFs@PDA. In addition, the energy dispersive spectrometer (EDS) elemental maps (Fig. S1) were utilized to present the components of g-C_3N_4-AuD@PPy and ZnONFs@PDA-sCuO. As shown in Fig. S1A, the existence of C, N and Au elements confirmed the uniform loading of AuD@PPy on g-C3N4. Fig. S1B showed the distribution of each element component in ZnONFs@PDA-sCuO, which proved the successful synthesis of ZnONFs@PDA-sCuO.

The phase composition of sCuO, ZnONFs and ZnONFs@PDA-sCuO was confirmed by XRD. In Fig. S2A, the peaks at 31.74°, 34.38°, 36.21°, 47.48°, 56.53° and 62.78° could be assigned to the planes of (100), (002), (101), (102), (110) and (103) of ZnONFs, respectively (JCPDS Card NO. 76–0704). The peaks at 35.45°, 35.56°, 38.74° and 38.93°corresponded to the planes of (002), (−111), (111) and (200) of sCuO, respectively (JCPDS Card No. 89–5897). Moreover, the characteristic peaks of both ZnONFs and sCuO were contained in the XRD pattern of ZnONFs@PDA-sCuO, manifesting the successful combination of ZnONFs@PDA and sCuO. In addition, the fourier transform infrared spectroscopy (FTIR) was used to analyze the characteristic groups of the obtained compounds. The absorption peaks of sCuO at 540 cm^{-1} were caused by the stretching vibration of Cu-O [42], which verifies its monoclinal structure (Fig. S2B). In the ZnO spectrum, the characteristic peak around 505 cm^{-1} was attributed to the Zn-O stretching vibration. In addition to the obvious absorption of Zn-O bond, the C═O stretching vibration in the template PVP leads to the characteristic peak around 1645 cm^{-1}. The peak of C-N stretching vibration at 1465 cm^{-1} and the peak of CH_2 groups on the pyrrole ring at 1381 cm^{-1} were also related to the template PVP. Additionally, the other characteristic functional groups of PVP were reflected at 908 cm^{-1} [43]. Moreover, the wide characteristic band at 3420 cm^{-1} was related to the O-H stretching vibration in the ZnO spectrum.

In the FTIR spectrum of PDA, the wide absorption band of 3400 cm^{-1} is O-H stretching vibration, the peaks at 1656 cm^{-1} and 1436 cm^{-1} correspond to C-C and phenolic C-O-H molecular vibration, respectively. And the absorption peak at 1125 cm^{-1} can be regarded as the N-H vibration in the heterocyclic ring. The FTIR spectrum of ZnONFs@PDA shows that the characteristic peaks of ZnONFs and PDA existed simultaneously, indicating that PDA was successfully modified onto the surface of the ZnONFs. Finally, the characteristic FTIR spectrum of ZnONFs@PDA-sCuO verified the effective loading of sCuO onto ZnONFs@PDA.

3.2. ECL mechanism

In order to explore the mechanism of the designed sensing system, the amplification and quenching strategies of ECL signal were illustrated

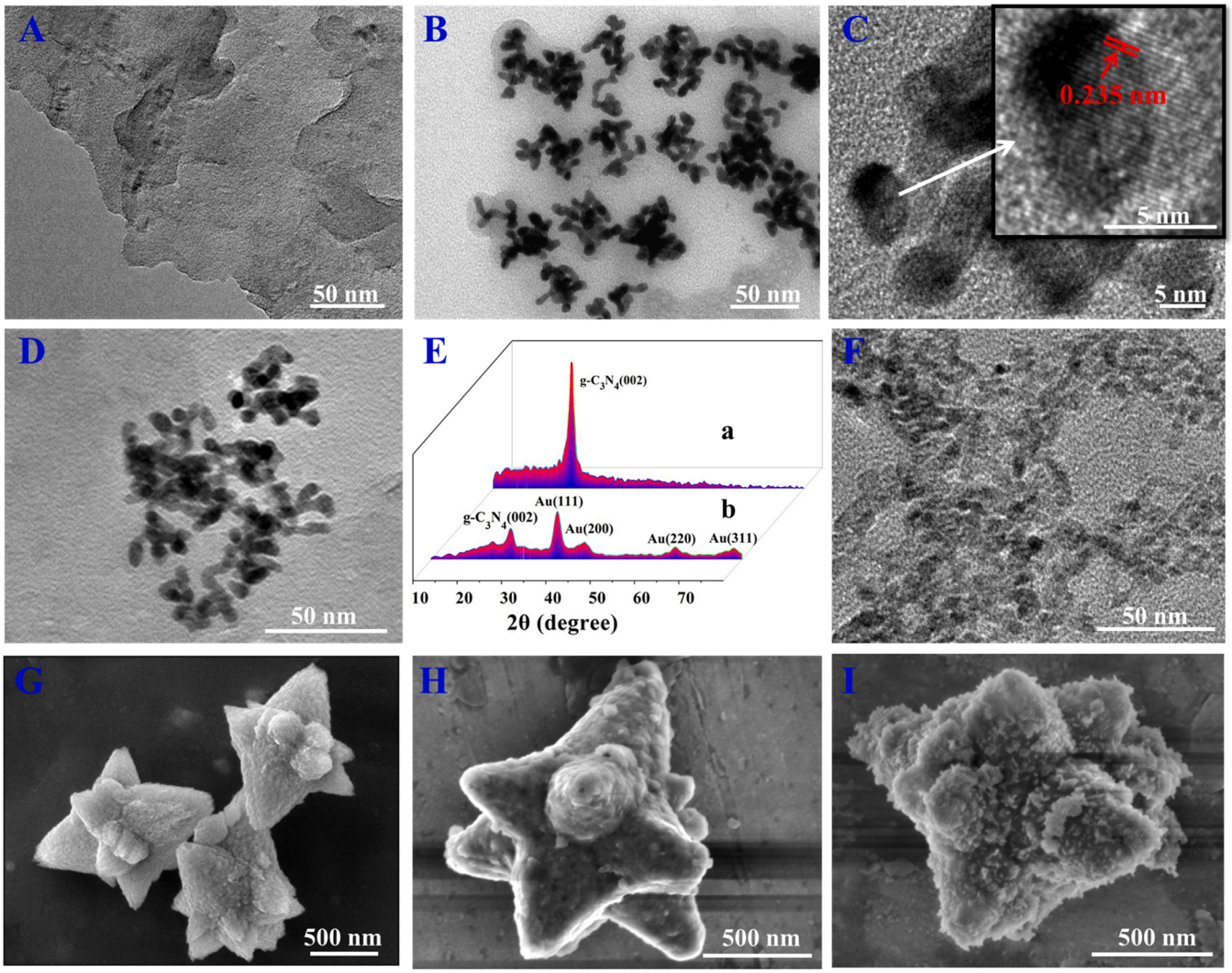

Fig. 1. TEM images of g-C_3N_4 NS (A) and AuD@PPy (B), HRTEM image of AuD@PPy (C), TEM image of g-C_3N_4-AuD@PPy (D), XRD (E) of g-C_3N_4 (a) and g-C_3N_4-AuD@PPy (b), TEM image of sCuO (F), SEM images of ZnONFs (G) and ZnONFs@PDA (H), ZnONFs@PDA-sCuO (I).

by control experiments. Fig. 2 A confirms that g-C_3N_4-AuD@PPy (curve b) has better ECL strength and stability than g-C_3N_4 (curve a). This is because gold dendrites also have good electroconductibility, which can improve transfer reaction rate of electron and enhance the ECL response stability of g-C_3N_4. According to the relevant literature, the possible ECL mechanisms were discussed [44]. When the electrode was scanned from − 1.5–0 V, g-C_3N_4 was rapidly converted to g-$C_3N_4^{\bullet-}$ by reduction reaction (Eq. 1). Simultaneously, $S_2O_8^{2-}$ lost electrons to transmute into $SO_4^{\bullet-}$ in the reaction process (Eq. 2). Then the reduction product $SO_4^{\bullet-}$ and g-$C_3N_4^{\bullet-}$ interacted to form g-C_3N_4 * (Eq. 3). Eventually, the unstable g-C_3N_4 * returned to the ground state, intense emission and light was released (Eq. 4).

$$g\text{-}C_3N_4 + e^- \rightarrow g\text{-}C_3N_4^{\bullet-} \quad (1)$$

$$S_2O_8^{2-} + e^- \rightarrow SO_4^{2-} + SO_4^{\bullet-} \quad (2)$$

$$g\text{-}C_3N_4^{\bullet-} + SO_4^{\bullet-} \rightarrow g\text{-}C_3N_4^{*} + SO_4^{2-} \quad (3)$$

$$g\text{-}C_3N_4^{*} \rightarrow g\text{-}C_3N_4 + h\nu \quad (4)$$

The quenching effect of ZnONFs@PDA-sCuO was also studied. As shown in Fig. 2B, ZnONFs@PDA was an effective quencher for g-C_3N_4-AuD@PPy, which might due to that the quinone units in the PDA could play a quenching role [38,45]. Furthermore, sCuO had obvious quenching rate as well. When combining ZnONFs@PDA and sCuO together, ZnONFs@PDA-sCuO was superior to either ZnONFs@PDA or sCuO for the quenching ability. Therefore, ZnONFs@PDA-sCuO can be applied as a double quencher for g-C_3N_4 ECL emission. More experiments have been conducted to explore the quenching mechanism. As can be seen from Fig. 2 C, when the ZnONFs@PDA surface was loaded with sCuO, the ultraviolet absorption intensity of ZnONFs@PDA-sCuO further increased, which helped to increase its effective overlap with the ECL emission spectrum of g-C_3N_4, thus it was much easier to conduct the ECL-RET interaction from g-C_3N_4-AuD@PPy (donor) to ZnONFs@PDA-sCuO (receptor). In addition, the overlapping region between each ultraviolet absorption curve and the ECL emission curve of Fig. 2 C were shown in Fig. S3A, and the corresponding overlapping area were also calculated and listed in Fig. S3B. The effective overlapping area of the ultraviolet absorption spectrum of ZnONFs@PDA-sCuO with the ECL emission spectrum of g-C_3N_4 were increased compared with that of ZnONFs@PDA.

To further investigate the performance of the ZnONFs@PDA-sCuO quencher, the ECL quenching test towards g-C_3N_4-AuD@PPy was explored by using a range of contents of ZnONFs@PDA-sCuO in PBS solution including 80 mM $K_2S_2O_8$. As shown in Fig. 2D, ECL intensity of g-C_3N_4-AuD@PPy was inversely proportional to the concentration of ZnONFs@PDA-sCuO. I_0 (ECL intensity without ZnONFs@PDA-sCuO)/I (ECL intensity with ZnONFs@PDA-sCuO) was linearly related to the concentrations of ZnONFs@PDA-sCuO with scope of 0 – 1.5 g L^{-1} (R^2 =

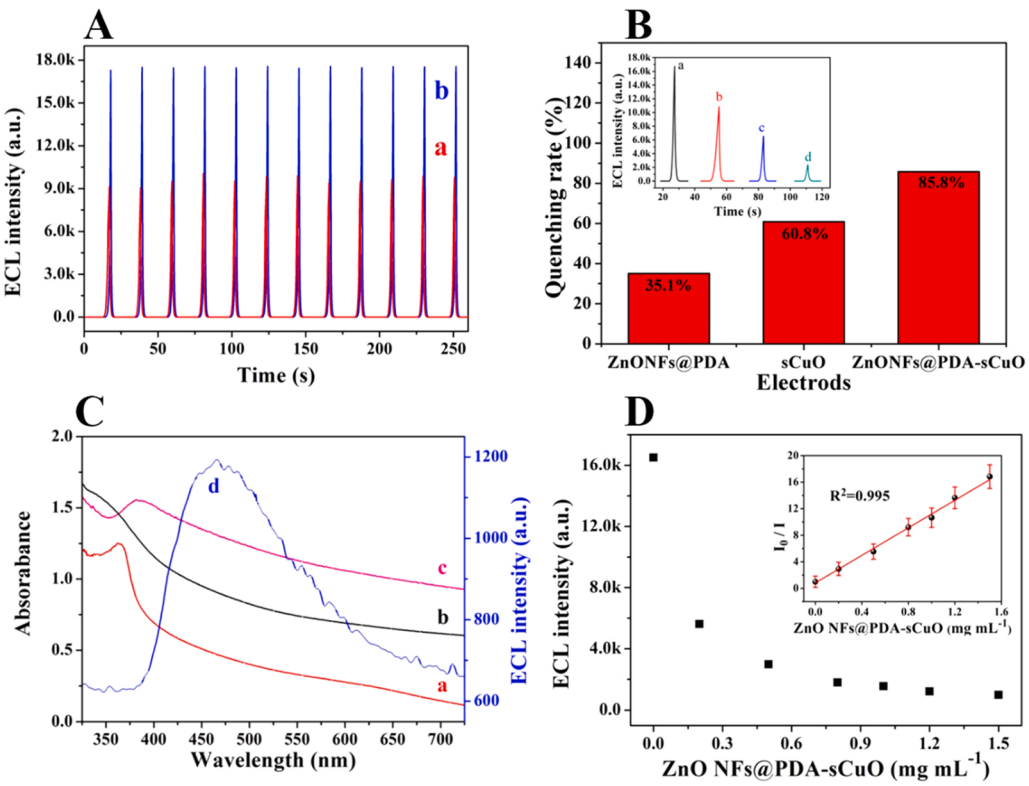

Fig. 2. (A) The ECL response of g-C_3N_4 (a), g-C_3N_4-AuD@PPy (b). (B) Quenching rate of ZnONFs@PDA, sCuO and ZnONFs@PDA-sCuO. The diagram inside corresponds to the ECL intensity of g-C_3N_4-AuD@PPy (a), the quenching effect of ZnONFs@PDA (b), sCuO (c) and ZnONFs@PDA-sCuO (d). (C) UV–vis absorption of ZnONFs@PDA (a), sCuO (b), ZnONFs@PDA-CuO (c) and the ECL emission spectrum of g-C_3N_4 (d). (D) ECL response of g-C_3N_4-AuD@PPy in the existing of 0, 0.2, 0.5, 0.8, 1, 1.2, and 1.5 mg mL^{-1} ZnONFs@PDA-sCuO; The internal graphic represents to linear relationship. Error bars = RSD ($n = 3$).

0.995), as shown in the inset of Fig. 2D. After fitting analysis and calculation, 1.037×10^6 g $^{-1}$ was obtained as the value of quenching constant (K_{sv}), which was evaluated in the light of the Stern-Volmer equation [46]. The excellent quenching effect of ZnONFs@PDA-sCuO was confirmed from all of the above results.

3.3. Optimization of the test conditions

Because the concentration of substrate, co-reactant and quencher and pH had a significant influence on the performance of the immunosensor, these conditions were explored in detail. Fig. 3A showed the

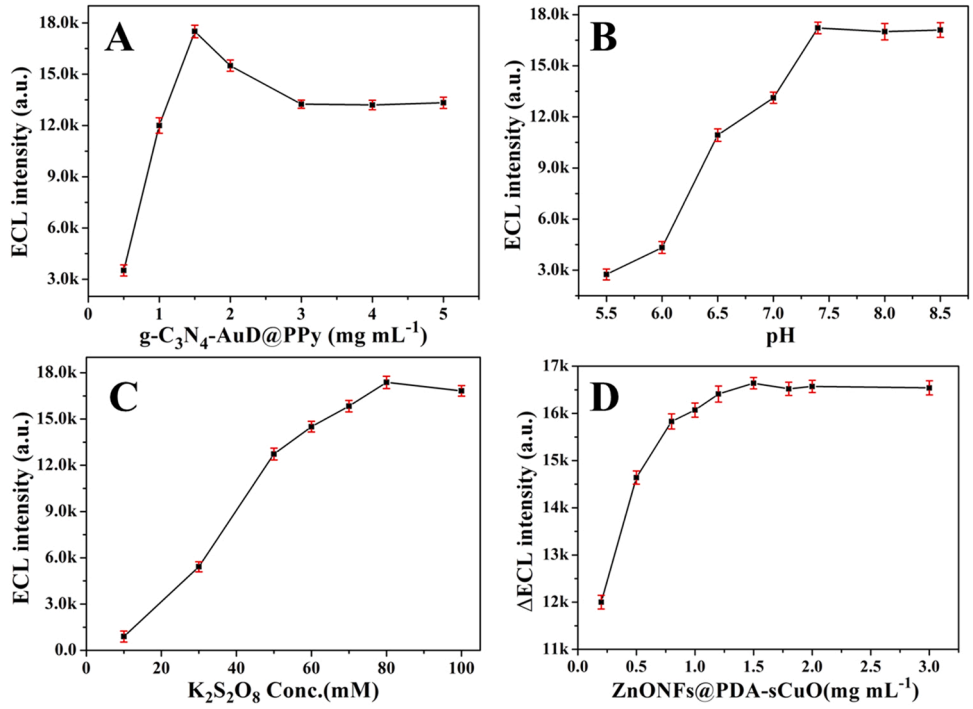

Fig. 3. The effect of concentration of g-C_3N_4-AuD@PPy (A), the pH of PBS solution (B) and the concentration of $K_2S_2O_8$ (C) on the ECL response from GCE/ g-C_3N_4-AuD@PPy. The quenching effect of ZnONFs@PDA-sCuO (ΔECL = GCE/g-C_3N_4-AuD@PPy /Ab_1/BSA/PCT - GCE/ g-C_3N_4-AuD@PPy /Ab_1/BSA/PCT/ ZnONFs@PDA-sCuO-Ab_2). Error bars = RSD ($n = 3$).

impact of the g-C_3N_4-AuD@PPy substrate. When the concentration of g-C_3N_4-AuD@PPy was below 1.5 mg mL^{-1}, the ECL response was in direct proportion to the concentration of g-C_3N_4-AuD@PPy. As the concentration of g-C_3N_4-AuD@PPy continues to increase, the signal intensity showed a slight downward trend. As a result, 1.5 mg mL^{-1} was the peak concentration on the curve, thus we defined it as the optimal g-C_3N_4-AuD@PPy concentration. In Fig. 3B, the ECL response increased with pH values ranging from 5.5 to 7.4. While the ECL.

signal showed a slight decline trend when the pH value increased from 7.4 to 8.5. Therefore, the most qualified pH value was chosen to be 7.4. Fig. 3C confirmed that the ECL strength of the system was closely related to the concentration of $K_2S_2O_8$, with a positive proportional increase relationship. ECL signal reached its maximum value at the concentration of 80 mM and did not increase significantly when the concentration continued to exceed 80 mM. Therefore, 80 mM $K_2S_2O_8$ could fully satisfy the test consumption and was determined as the best co-reaction agent condition. Fig. 3D confirmed that the change of quenching agent concentration had a significant influence on the intensity of ECL signal in the system. When the concentration of ZnONFs@PDA-sCuO reached 1.5 mg mL^{-1}, which matched with the concentration of the substrate luminescent material to achieve the best quenching effect. Therefore, the optimal quencher concentration was 1.5 mg mL^{-1}.

3.4. Characterization of the immunosensor

The characteristics between ECL strength and voltage of different modified electrodes in the construction process was used to verify that the immunosensor was successfully fabricated, and the consequences were displayed in Fig. 4 A. The undecorated working electrode generated a weak ECL signal (curve a). The g-C_3N_4-AuD@PPy was excited at the working electrode and showed a significant ECL response (curve b). Because the high impedance of proteins could hinder electron transfer, so the ECL intensity in the system was gradually reduced after modifying Ab_1, dripping BSA and casting PCT onto the working electrode, successively (curve c to curve e). When ZnONFs@PDA-sCuO-Ab_2 was continued to be added, the electrode suffered a significant ECL inhibition (curve f), indicating the high quenching efficiency of the quenching label ZnONFs@PDA-sCuO-Ab_2. The results showed that the immunosensor was successfully manufactured by layered modification.

Furthermore, electrochemical impedance spectroscopy (EIS) test on different modified electrodes strongly demonstrated the constructed sensing platform. As shown in Fig. 4B, the diameter of the curve in the EIS spectrum represented the strength of the electron transfer resistance (R_{et}), which reflected the diffusion retardation of the electroactive marker at the electrode interface. The results showed that the electron transfer of the unmodified GCE was almost unimpeded and thus curve a appears as a minuscule semicircle in the EIS spectrum. Curve b was a small semicircle on the EIS spectrum, indicating that the impedance value of the electrode modified by g-C_3N_4-AuD@PPy was low, which confirmed that Au dendrites gave excellent conductivity to the substrate material. The Ab_1, BSA and PCT (curve c to curve e) were continuously modified on the electrode surface, and the impedance values progressively increased in EIS spectrum, because these substances hindered electron transfer as nonelectroactive substances. Finally, when the working electrode was modified with ZnONFs@PDA-sCuO-Ab_2, the R_{et} value reached the maximum (curve f), confirming that the immunoreactions occurred between PCT antigen and Ab_2 biological conjugate. The experimental results fully proved that the proposed immunosensor was successfully constructed. ZSimpWin software was used for simulation analysis of the proposed sensor strategy, and the specific simulation values were shown in Table S1.

3.5. Analytical performance of the immunosensor

The working performance of the immunosensor was usually determined by the ECL strength of PCT at different concentrations as evaluation indexes, so the working curve of the sensor can be measured under the optimum test parameters. As depicted in Fig. 4 C, in the PCT concentration range of 0.00005–50 ng mL^{-1}, the ECL intensity of the

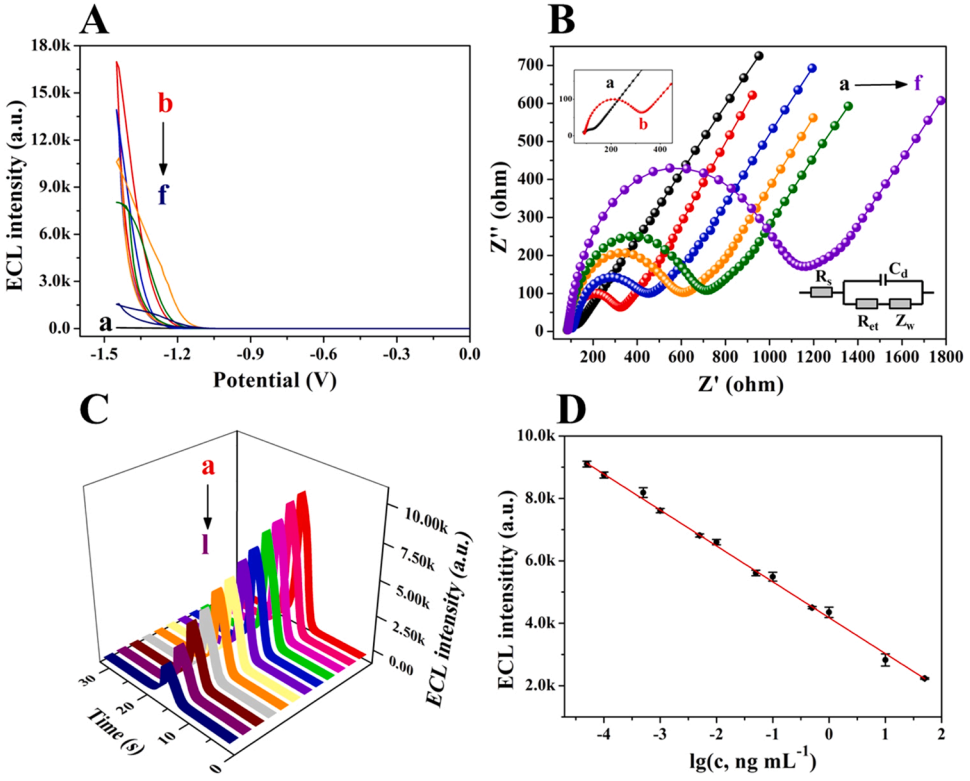

Fig. 4. (A) The ECL intensity-potential curves and (B) the corresponding EIS of GCE (a), GCE/g-C_3N_4-AuD@PPy (b), GCE/g-C_3N_4-AuD@PPy/Ab_1 (c), GCE/g-C_3N_4-AuD@PPy/Ab_1/BSA (d), GCE/g-C_3N_4-AuD@PPy/Ab_1/BSA/PCT (e), GCE/g-C_3N_4-AuD@PPy/Ab_1/BSA/PCT/ZnONFs@PDA-sCuO-Ab_2 (f). (C) The ECL response of immunosensors to detect a range of concentrations of PCT, from a to l: 0.00005, 0.0001, 0.0005, 0.001, 0.005, 0.01, 0.05, 0.1, 0.5, 1, 10 and 50 ng mL^{-1}. (D) The corresponding calibration curve. Error bars = RSD ($n = 3$).

quench-type sensor was gradually reduced by biological immune recognition. According to the test results, the calibration curve of the sensor was obtained by fitting analysis, the linear regression equation $I_{ECL} = 4179.39–1167.65 \times \lg c$ with a correlation coefficient of 0.997 was reliable (Fig. 4D). The performance of the proposed sensor in this work was better than that of other analysis strategies of the same type (Table S2), the superior linear detection range was 0.00005–50 ng mL^{-1} and the detection limit was 17.2 fg mL^{-1} (S/N = 3), which might originate from that g-C_3N_4-AuD@PPy has significant ECL emission property and ZnONFs@PDA-sCuO has prominent quenching performance.

3.6. Application performance of the immunosensor

Protein markers similar to the target antigen were usually used as interfering substances to evaluate the specificity of immunosensors. Alpha fetoprotein (AFP), human serum albumin (HSA), prostate specific antigen (PSA), BSA, immunoglobulin G (IgG) and carcinoembryonic antigen (CEA) were common antigens in our choice of interfering substances. As shown in Fig. 5 A, when the detection object contained only one of the aforementioned interferents, the ECL intensity showed no obvious change compared with the blank experiment. Furthermore, when the detection system only contained PCT antigen or mixed PCT with other interfering substances, the sensing system could induce immune response to significantly quench the ECL signals. The above results indicated an acceptable selectivity specificity of this ECL immunosensor.

The repeatability of the proposed sensor was systematically researched by repetitive experiment. Specifically, the ECL behavior of five immunosensors of the same batch and five batches of sensors constructed on the same electrode were investigated respectively under the same test conditions. The experimental results showed that the RSD values of the two groups were satisfactory, which were 2.32% and 1.45%, respectively, confirming that the immunosensor has excellent repeatability (Fig. 5B).

Stability is one of the important application performances of immunosensor, and thus superior stability is beneficial to the practical operation of immunosensor. As shown in Fig. 5 C, in order to prove the stability of the prepared immunosensor, the working electrode was continuously scanned by cyclic potential for 12 times. The experimental results showed that the ECL signal strength of the sensor used for testing 0.1 ng mL^{-1} PCT was generally stable under continuous voltage scanning, and the calculated RSD value was 1.24%, which fully proved that the sensor had outstanding stability.

3.7. Practical application in human serum

The recovery of serum samples needs to be considered in the practical application of ECL immunosensor. In order to evaluate the reliability of the proposed sensor for PCT detection, the recovery rate was analyzed by standard addition method in this work. The biosensor constructed in this study was used to measure serum samples, and the concentration of PCT in serum was 0.33 ng mL^{-1} (denoted as detection concentration). The recovery analysis results displayed in Table 1 was 96.8–104%, which confirmed that the proposed immunosensor with superb performance can perform clinical samples detection well.

4. Conclusion

In brief, a quench-type ECL biosensor has been developed based on the ECL-RET interaction between g-C_3N_4-AuD@PPy donor and ZnONFs@PDA-sCuO acceptor to realize ultrasensitive analysis of PCT. In this system, monodisperse gold dendrite@polypyrrole core–shell nanoparticles were applied to improve the ECL performance of g-C_3N_4, resulting in a high-efficiency signal probe g-C_3N_4-AuD@PPy. Meanwhile, small-sized CuO nanoparticles and PDA modified ZnO nanoflowers were innovatively combined to achieve efficient quenching, which significantly improved the sensitivity of the biosensor. Furthermore, the results showed that the biosensor had superior linear detection range from 0.00005 to 50 ng mL^{-1}, and the detection limit was 17.2 fg mL^{-1} (S/N = 3). In addition, the biosensor has excellent stability, repeatability and selectivity. Therefore, this novel analytical method showed predictable application benefits in the identification of serious diseases.

CRediT authorship contribution statement

Tengfei Shi, Lihua Hu, and Yuyang Li conceived and designed the experiments. **Tengfei Shi** performed the experiments, analyzed the data and wrote the original draft of the manuscript. **Lihua Hu** analyzed the data and revised the manuscript. **Jiye Chen, Qianqian Cui, Hao Yu, Dan Wu, Hongmin Ma, Qin Wei and Huangxian Ju** contributed substantially to revisions. All the authors discussed the results and commented on the manuscript.

Table 1
The recovery analysis results.

Sample number	Detected concentration (ng mL^{-1})	Addition (ng mL^{-1})	Found (ng mL^{-1})	Recovery (%)	RSD (%, $n = 3$)
1	0.330	1.00	1.298	96.8	2.8
2	0.330	0.100	0.434	104	3.4
3	0.330	0.050	0.381	102	5.1
4	0.330	0.010	0.331	100	3.6

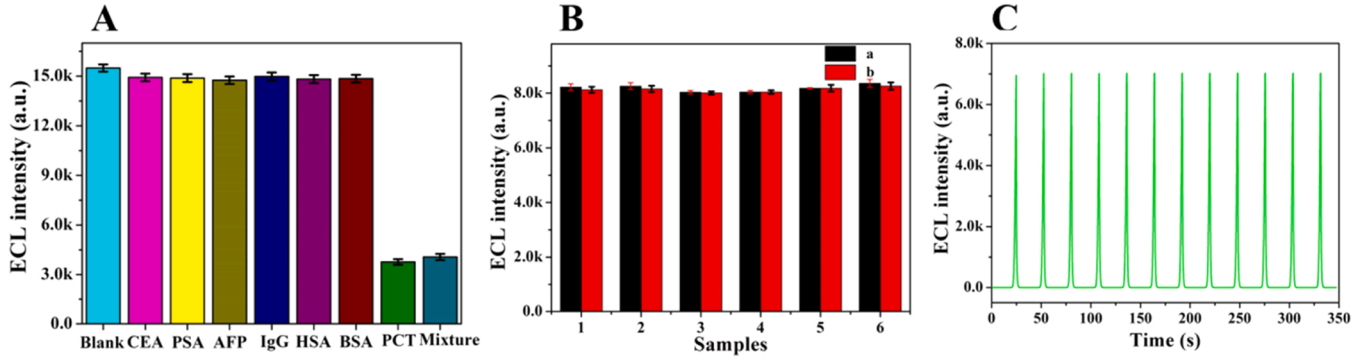

Fig. 5. (A) The ECL intensity responses of the biosensors to separate 10 ng mL^{-1} CEA, PSA, AFP, IgG, HSA, BSA and 1 ng mL^{-1} PCT. The mixture refers to the mixing of CEA, PSA, AFP, IgG, HSA, BSA and PCT. Error bars = RSD ($n = 3$), (B) The repeatability of the proposed sensor was systematically researched by repetitive experiment with intra- (a) and inter-assay (b). Error bars = RSD ($n = 3$), (C) The stability of the ECL immunosensor for 12 cycles.

Declaration of Competing Interest

The authors declare that they have no known competing financial interests or personal relationships that could have appeared to influence the work reported in this paper.

Data availability

No data was used for the research described in the article.

Acknowledgements

This study was supported by the National Natural Science Foundation of China [Nos. 21607055, 21675063, 21775054, 21505051, 21575050, 21777056], National Key Scientific Instrument and Equipment Development Project of China [No.21627809].

Appendix A. Supporting information

Supplementary data associated with this article can be found in the online version at doi:10.1016/j.snb.2022.132591.

References

[1] X. Xu, X. Song, R. Nie, Y. Yang, Y. Chen, L. Yang, Ultra-sensitive capillary immunosensor combining porous-layer surface modification and biotin-streptavidin nano-complex signal amplification: application for sensing of procalcitonin in serum, Talanta 205 (2019), 120089, https://doi.org/10.1016/j.talanta.2019.06.089.

[2] B. Ran, W. Zheng, M. Dong, Y. Xianyu, Y. Chen, J. Wu, Z. Qian, X. Jiang, Peptide-mediated controllable cross-linking of gold nanoparticles for immunoassays with tunable detection Range, Anal. Chem. 90 (2018) 8234–8240, https://doi.org/10.1021/acs.analchem.8b01760.

[3] W.J. Shen, Y. Zhuo, Y.Q. Chai, Z.H. Yang, J. Han, R. Yuan, Enzyme-free electrochemical immunosensor based on host-guest nanonets catalyzing amplification for procalcitonin detection, ACS Appl. Mater. Inter. 7 (2015) 4127–4134, https://doi.org/10.1021/am508137t.

[4] C. Tascini, A. Aimo, C. Arzilli, F. Sbrana, A. Ripoli, L. Ghiadoni, C. Bertone, C. Passino, V. Attanasio, E. Sozio, E. Taddei, R. Murri, M. Fantoni, F. Paciosi, D. Francisci, M.B. Pasticci, C. Pallotto, G.Di Caprio, A. Carozza, S. Maffei, M. Emdin, Procalcitonin, white blood cell count and C-reactive protein as predictors of S. aureus infection and mortality in infective endocarditis, Int. J. Cardiol. 301 (2020) 190–194, https://doi.org/10.1016/j.ijcard.2019.08.013.

[5] H. Xiao, P. Zhang, Y. Xiao, H. Xiao, M. Ma, C. Lin, J. Luo, H. Quan, K. Tao, G. Huang, Diagnostic accuracy of procalcitonin as an early predictor of infection after radical gastrectomy for gastric cancer: a prospective bicenter cohort study, Int. J. Surg. 75 (2020) 3–10, https://doi.org/10.1016/j.ijsu.2020.01.019.

[6] F. Bonelli, V. Meucci, T.J. Divers, A. Boccardo, D. Pravettoni, M. Meylan, A. G. Belloli, M. Sgorbini, Plasma procalcitonin concentration in healthy calves and those with septic systemic inflammatory response syndrome, Vet. J. 234 (2018) 61–65, https://doi.org/10.1016/j.tvjl.2018.02.003.

[7] S. Dhampalwar, A. Borkakoty, S. Taneja, A. Duseja, R.K. Dhiman, Y.K. Chawla, Role of procalcitonin in early detection of infections in acute on chronic liver failure in liver intensive care, J. Clin. Exp. Hepatol. 6 (2016) S7, https://doi.org/10.1016/j.jceh.2016.06.013.

[8] K. Berge, M.N. Lyngbakken, G. Einvik, J.A. Winther, J. Brynildsen, R. Røysland, H. Strand, G. Christensen, A.D. Høiseth, T. Omland, H. Røsjø, Diagnostic and prognostic properties of procalcitonin in patients with acute dyspnea: Data from the ACE 2 Study, Clin. Biochem 59 (2018) 62–68, https://doi.org/10.1016/j.clinbiochem.2018.07.006.

[9] R. Pyati, M.M. Richter, ECL—Electrochemical luminescence, Annu. Rep. Prog. Chem., Sect. C: Phys. Chem. 103 (2007) 12–78, https://doi.org/10.1039/b605635k.

[10] Y. Zhang, F. Wang, H. Zhang, H. Wang, Y. Liu, Multivalency interface and g-C_3N_4 coated liquid metal nanoprobe signal amplification for sensitive electrogenerated chemiluminescence detection of exosomes and their surface proteins, Anal. Chem. 91 (2019) 12100–12107, https://doi.org/10.1021/acs.analchem.9b03427.

[11] S. Bozorgzadeh, B. Haghighi, Enhanced electrochemiluminescence of ZnO nanoparticles decorated on multiwalled carbon nanotubes in the presence of peroxydisulfate, Microchim. Acta 183 (2016) 1487–1492, https://doi.org/10.1007/s00604-016-1785-8.

[12] Z. Fan, Z. Lin, Z. Wang, J. Wang, M. Xie, J. Zhao, K. Zhang, W. Huang, Dual-wavelength electrochemiluminescence ratiometric biosensor for nf-kappab p50 detection with dimethylthiodiaminoterephthalate fluorophore and self-assembled DNA tetrahedron nanostructures probe, ACS Appl. Mater. Inter. 12 (2020) 11409–11418, https://doi.org/10.1021/acsami.0c01243.

[13] Z. Guo, L. Wu, Y. Hu, S. Wang, X. Li, Potential-resolved "in-electrode" type electrochemiluminescence immunoassay based on functionalized g-C_3N_4 nanosheet and Ru-NH_2 for simultaneous determination of dual targets, Biosens. Bioelectron. 95 (2017) 27–33, https://doi.org/10.1016/j.bios.2017.03.013.

[14] Z.H. Xu, H. Wang, J. Wang, W. Zhao, J.J. Xu, H.Y. Chen, Bidirectional electrochemiluminescent sensing: an application in detecting miRNA-141, Anal. Chem. 91 (2019) 12000–12005, https://doi.org/10.1021/acs.analchem.9b02914.

[15] B. Babamiri, A. Salimi, R. Hallaj, Switchable electrochemiluminescence aptasensor coupled with resonance energy transfer for selective attomolar detection of Hg^{2+} via CdTe@CdS/dendrimer probe and Au nanoparticle quencher, Biosens. Bioelectron. 102 (2018) 328–335, https://doi.org/10.1016/j.bios.2017.11.034.

[16] H.J. Lu, J.B. Pan, Y.Z. Wang, S.Y. Ji, W. Zhao, X.L. Luo, J.J. Xu, H.Y. Chen, Electrochemiluminescence energy resonance transfer system between RuSi nanoparticles and hollow Au nanocages for nucleic acid detection, Anal. Chem. 90 (2018) 10434–10441, https://doi.org/10.1021/acs.analchem.8b02347.

[17] M.S. Wu, L.J. He, J.J. Xu, H.Y. Chen, RuSi@Ru(bpy)$_3^{2+}$/Au@Ag_2S nanoparticles electrochemiluminescence resonance energy transfer system for sensitive DNA detection, Anal. Chem. 86 (2014) 4559–4565, https://doi.org/10.1021/ac500591n.

[18] Z. Zhou, Y. Zhang, Y. Shen, S. Liu, Y. Zhang, Molecular engineering of polymeric carbon nitride: advancing applications from photocatalysis to biosensing and more, Chem. Soc. Rev. 47 (2018) 2298–2321, https://doi.org/10.1039/c7cs00840f.

[19] Y. Zheng, Y. Jiao, J. Chen, J. Liu, J. Liang, A. Du, W. Zhang, Z. Zhu, S.C. Smith, M. Jaroniec, G.Q. Lu, S.Z. Qiao, Nanoporous graphitic-C_3N_4@carbon metal-free electrocatalysts for highly efficient oxygen reduction, J. Am. Chem. Soc. 133 (2011) (2011) 6–20119, https://doi.org/10.1021/ja209206c.

[20] N. Rahbar, Z. Salehnezhad, A. Hatamie, A. Babapour, Graphitic carbon nitride nanosheets as a fluorescent probe for chromium speciation, Mikrochim. Acta 185 (2018) 101, https://doi.org/10.1007/s00604-017-2615-3.

[21] A. Ahmed, P. John, M.H. Nawaz, A. Hayat, M. Nasir, Zinc-doped mesoporous graphitic carbon nitride for colorimetric detection of hydrogen peroxide, ACS Appl. Nano Mater. 2 (2019) 5156–5168, https://doi.org/10.1021/acsanm.9b01036.

[22] C. Cheng, Y. Huang, X. Tian, B. Zheng, Y. Li, H. Yuan, D. Xiao, S. Xie, M.M. Choi, Electrogenerated chemiluminescence behavior of graphite-like carbon nitride and its application in selective sensing Cu^{2+}, Anal. Chem. 84 (2012) 4754–4759, https://doi.org/10.1021/ac300205w.

[23] Y. Wang, Y. Zhang, H. Sha, X. Xiong, N. Jia, Design and biosensing of a ratiometric electrochemiluminescence resonance energy transfer aptasensor between a g-C_3N_4 nanosheet and Ru@MOF for Amyloid-beta protein, ACS Appl. Mater. Inter. 11 (2019) 36299–36306, https://doi.org/10.1021/acsami.9b09492.

[24] L. Yu, Q. Zhang, Q. Kang, B. Zhang, D. Shen, G. Zou, Near-infrared electrochemiluminescence immunoassay with biocompatible Au nanoclusters as tags, Anal. Chem. 92 (2020) 7581–7587, https://doi.org/10.1021/acs.analchem.0c00125.

[25] X. Zhang, W. Li, Y. Zhou, Y. Chai, R. Yuan, An ultrasensitive electrochemiluminescence biosensor for MicroRNA detection based on luminol-functionalized Au NPs@ZnO nanomaterials as signal probe and dissolved O_2 as coreactant, Biosens. Bioelectron. 135 (2019) 8–13, https://doi.org/10.1016/j.bios.2019.04.004.

[26] C. Wang, M. Chen, J. Wu, F. Mo, Y. Fu, Multi-functional electrochemiluminescence aptasensor based on resonance energy transfer between Au nanoparticles and lanthanum ion-doped cadmium sulfide quantum dots, Anal. Chim. Acta 1086 (2019) 66–74, https://doi.org/10.1016/j.aca.2019.08.012.

[27] Y. Yu, C. Lu, M. Zhang, Gold nanoclusters@Ru(bpy)$_3^{2+}$-layered double hydroxide ultrathin film as a cathodic electrochemiluminescence resonance energy transfer probe, Anal. Chem. 87 (2015) 8026–8032, https://doi.org/10.1021/acs.analchem.5b02208.

[28] W. Hu, H. Chen, C.M. Li, One-step synthesis of monodisperse gold dendrite@polypyrrole core-shell nanoparticles and their enhanced catalytic durability, Colloid Polym. Sci. 293 (2014) 505–512, https://doi.org/10.1007/s00396-014-3440-4.

[29] L. Hao, C. Zhu, C. Chen, P. Kang, Y. Hu, W. Fan, Z. Chen, Fabrication of silica core–conductive polymer polypyrrole shell composite particles and polypyrrole capsule on monodispersed silica templates, Synth. Met. 139 (2003) 391–396, https://doi.org/10.1016/s0379-6779(03)00193-0.

[30] Q. Han, C. Wang, Z. Li, J. Wu, P.K. Liu, F. Mo, Y. Fu, Multifunctional zinc oxide promotes electrochemiluminescence of porphyrin aggregates for ultrasensitive detection of copper ion, Anal. Chem. 92 (2020) 3324–3331, https://doi.org/10.1021/acs.analchem.9b05262.

[31] D. Liu, L. Wang, S. Ma, Z. Jiang, B. Yang, X. Han, S. Liu, A novel electrochemiluminescent immunosensor based on CdS-coated ZnO nanorod arrays for HepG2 cell detection, Nanoscale 7 (2015) 3627–3633, https://doi.org/10.1039/c4nr06946c.

[32] A. Chen, S. Ma, Y. Zhuo, Y. Chai, R. Yuan, In situ electrochemical generation of electrochemiluminescent silver naonoclusters on target-cycling synchronized rolling circle amplification platform for MicroRNA detection, Anal. Chem. 88 (2016) 3203–3210, https://doi.org/10.1021/acs.analchem.5b04578.

[33] M. Xiong, Q. Rong, H.M. Meng, X.B. Zhang, Two-dimensional graphitic carbon nitride nanosheets for biosensing applications, Biosens. Bioelectron. 89 (2017) 212–223, https://doi.org/10.1016/j.bios.2016.03.043.

[34] L. Xu, J. Su, G. Zheng, L. Zhang, Enhanced photocatalytic performance of porous ZnO thin films by CuO nanoparticles surface modification, Mat. Sci. Eng. B. 248 (2019), https://doi.org/10.1016/j.mseb.2019.114405.

[35] W. Hu, G. He, H. Zhang, X. Wu, J. Li, Z. Zhao, Y. Qiao, Z. Lu, Y. Liu, C.M. Li, Polydopamine-functionalization of graphene oxide to enable dual signal amplification for sensitive surface plasmon resonance imaging detection of biomarker, Anal. Chem. 86 (2014) 4488–4493, https://doi.org/10.1021/ac5003905.

[36] Y. Liu, M.A. Haghighatbin, W. Shen, H. Cui, Functionalized polydopamine nanospheres with chemiluminescence and immunoactivity for label-free copeptin immunosensing, ACS Appl. Nano Mater. 3 (2020) 4681–4689, https://doi.org/10.1021/acsanm.0c00682.
[37] X. Chen, Y. Yan, M. Müllner, M.P. van Koeverden, K.F. Noi, W. Zhu, F. Caruso, Engineering fluorescent poly(dopamine) capsules, Langmuir 30 (2014) 2921–2925, https://doi.org/10.1021/la4049133.
[38] Y. Zhao, L. Li, L. Hu, Y. Zhang, D. Wu, H. Ma, Q. Wei, An electrochemiluminescence immunosensor for the N-terminal brain natriuretic peptide based on the high quenching ability of polydopamine, Microchim. Acta 186 (2019) 606, https://doi.org/10.1007/s00604-019-3709-x.
[39] H. Sha, Y. Zhang, Y. Wang, H. Ke, X. Xiong, N. Jia, Electrochemiluminescence resonance energy transfer biosensor between the glucose functionalized MnO_2 and g-C_3N_4 nanocomposites for ultrasensitive detection of concanavalin A, Biosens. Bioelectron. 124- 125 (2019) 59–65, https://doi.org/10.1016/j.bios.2018.10.023.
[40] Y. Xu, X.B. Yin, X.W. He, Y.K. Zhang, Electrochemistry and electrochemiluminescence from a redox-active metal-organic framework, Biosens. Bioelectron. 68 (2015) 197–203, https://doi.org/10.1016/j.bios.2014.12.031.
[41] A.L. Hu, H.H. Deng, X.Q. Zheng, Y.Y. Wu, X.L. Lin, A.L. Liu, X.H. Xia, H.P. Peng, W. Chen, G.L. Hong, Self-cascade reaction catalyzed by CuO nanoparticle-based dual-functional enzyme mimics, Biosens. Bioelectron. 97 (2017) 21–25, https://doi.org/10.1016/j.bios.2017.05.037.
[42] İ.Y. Erdoğan, Ö. Güllü, Optical and structural properties of CuO nanofilm: its diode application, J. Alloy Compod. 492 (2010) 378–383, https://doi.org/10.1016/j.jallcom.2009.11.109.
[43] S. Selvam, M. Sundrarajan, Functionalization of cotton fabric with PVP/ZnO nanoparticles for improved reactive dyeability and antibacterial activity, Carbohyd. Polym. 87 (2012) 1419–1424, https://doi.org/10.1016/j.carbpol.2011.09.025.
[44] X. Zhou, W. Zhang, Z. Wang, J. Han, G. Xie, S. Chen, Ultrasensitive aptasensing of insulin based on hollow porous $C_3N_4/S_2O_8^{2-}$/AuPtAg ECL ternary system and DNA walker amplification, Biosens. Bioelectron. 148 (2020), 111795, https://doi.org/10.1016/j.bios.2019.111795.
[45] Y. Liu, Y. Zhao, Z. Zhu, Z. Xing, H. Ma, Q. Wei, Ultrasensitive immunosensor for prostate specific antigen using biomimetic polydopamine nanospheres as an electrochemiluminescence superquencher and antibody carriers, Anal. Chim. Acta 963 (2017) 17–23, https://doi.org/10.1016/j.aca.2017.01.068.
[46] J. Xue, L. Yang, Y. Jia, Y. Zhang, D. Wu, H. Ma, L. Hu, Q. Wei, H. Ju, Dual-quenching electrochemiluminescence resonance energy transfer system from Ru-In_2S_3 to alpha-MoO_3-Au based on protect of protein bioactivity for procalcitonin detection, Biosens. Bioelectron. 142 (2019), 111524, https://doi.org/10.1016/j.bios.2019.111524.

Tengfei Shi studies in school of chemistry and chemical engineering, University of Jinan as postgraduate student.

Lihua Hu received her Ph.D. degree from University of science and technology of China in 2011. Now, she is an associate professor at University of Jinan. Her main research interests focus on the determination of biological targets through chemical sensors.

Jiye Chen studies in school of chemistry and chemical engineering, University of Jinan as undergraduate student.

Qianqian Cui studies in school of chemistry and chemical engineering, University of Jinan as postgraduate student.

Hao Yu studies in school of chemistry and chemical engineering, University of Jinan as postgraduate student.

Yuyang Li received his Ph.D. degree from China University of Petroleum (East China) in 2018. His main research interest are the design and preparation of functional nanomaterial, sensor technology, fluorescence imaging, and their industrial application. He has been hosting one national scientific research project.

Dan Wu received the D.S. degree from Shandong University in 2005. Now, she is a professor at University of Jinan. She dedicates to the surfactant and biological macromolecules interaction. And now she also studies the role of surfactant in electrochemical immunosensor.

Hongmin Ma received both his B.S. and M.S. degree in Applied Chemistry from University of Jinan in 2005 and 2008 respectively. And he has received his Ph.D. degree in Colloid and Interface Chemistry at Shandong University, investigating self-assembly at all scales at surfaces in 2011. Now, he is a professor at University of Jinan, interested in the assembly of nano-composites and the construction of ordered porous films as well as their analytical applications.

Qin Wei, a professor and DSc, has devoted herself to analytical teaching and scientific research. Her main research interests are the determination of protein and nucleic acid by photometry and the electrochemical immunosensor preparation. She has published over one hundred articles on analysis, immunosensor and applied successfully for many research projects, such as *Biomaterials, Adv. Funct. Mater., Biosens. Bioelectron., Sens. Actuators B: Chem., Talanta.*

Huangxian Ju received his BS, MS and PhD degrees from Nanjing University during 1982–1992, and was a postdoc in Montreal University (Canada) in 1996–1997. He became an associate and full professor of Nanjing University in 1993 and 1999. He is currently the director of State Key Laboratory of Analytical Chemistry for Life Science, Professor of Nanjing University and University of Jinan. His research interests focus on analytical biochemistry, biosensing and molecular diagnosis. He has authored 75 patents (39 approved), 6 English books, 7 Chinese books and 20 chapters, and published 786 papers in different journals with h-index of 100 (Google Scholar h-index 109 with more than 44000 citations).